Supporting Information: Exploitable magnetic anisotropy of the two-dimensional magnet CrI_3

Jeongwoo Kim[†], Kyoung-Whan Kim[‡], Bumseop Kim[§], Chang-Jong Kang[||], Dongbin Shin[§], Sang-Hoon Lee[⊥], Byoung-Chul Min[‡] & Noejung Park[*,§]

[†]*Department of Physics, Incheon National University, Incheon 22012, Korea*

[‡]*Center for Spintronics, Korea Institute of Science and Technology, Seoul 02792, Korea*

[§]*Department of Physics, Ulsan National Institute of Science and Technology, UNIST-gil 50, Ulsan 44919, Korea*

[||]*Department of Physics and Astronomy, Rutgers University, Piscataway, New Jersey 08854, USA*

[⊥]*Korea Institute for Advanced Study, Seoul 02455, Korea*

J. Kim and K.-W. Kim equally contributed to this work.

Corresponding Author

*E-mail : noejung@unist.ac.kr, Phone +82-10-7674-3211,+49-01773323991

Supporting Information

Figures S1-S7

Analytic theory for the direct and indirect SOC effect in the CrI_3 monolayer

We show that the spin-orbit coupling (SOC) Hamiltonian, including the ligand effect, for the spin states of the Cr atom can be written as $H_{\mathrm{SOC}} = \xi_1 \mathbf{S}^{\mathrm{Cr}} \cdot \mathbf{L}^{\mathrm{Cr}} + \xi_2 \mathbf{S}^{\mathrm{Cr}} \cdot \mathbf{L}^{\mathrm{I}}$. The first term represents the conventional atomic SOC at the Cr atomic site. To derive the second term, we need to start from the block-diagonal form of the tight-binding Hamiltonian.

$$H_2 = \begin{pmatrix} H_{\mathrm{Cr}} & H_{\mathrm{hop}} \\ H_{\mathrm{hop}}^{\dagger} & H_{\mathrm{I}} \end{pmatrix}, \tag{S1}$$

where H_{X} indicates the onsite Hamiltonian in X atoms, and H_{hop} is the hopping term between the two atomic species. Each of the block matrices consists of spin and orbital states of each of the atomic sites.

Among the parameters in this consideration, the energy gap between the conduction (Cr) and the valance bands (I) (See Figure S1a) is the largest one, and thus the other energy scales can be perturbatively treated. Here, we focus on the effect of the SOC in I atom, and the other smaller energy scales are ignored. We regard the Cr Hamiltonian as the onsite energy $H_{\mathrm{Cr}} \approx \epsilon_{\mathrm{Cr}}$, and the block-diagonal Hamiltonian for I can be inferred as the sum of the onsite energy and SOC $H_{\mathrm{I}} \approx \epsilon_{\mathrm{I}} + \eta_{\mathrm{I}} \mathbf{S} \cdot \mathbf{L}^{\mathrm{I}}$, where η_{I} is the SOC constant in I atoms.

To project Eq. (S1) to the Cr subspace, we define the unperturbed Hamiltonian $H_2^0 = \begin{pmatrix} H_{\mathrm{Cr}} & 0 \\ 0 & H_{\mathrm{I}} \end{pmatrix}$ and take the Schrieffer–Wolff transformation with respect to the perturbing Hamiltonian $V = \begin{pmatrix} 0 & H_{\mathrm{hop}} \\ H_{\mathrm{hop}}^{\dagger} & 0 \end{pmatrix}$. First, we sought an anti-unitary matrix S satisfying $[H_2^0, S] = V$. After some algebra, we obtain

$$S = \begin{pmatrix} 0 & H_{\mathrm{hop}}\left(\Delta E_{\mathrm{gap}} - \eta_{\mathrm{I}} \mathbf{S} \cdot \mathbf{L}^{\mathrm{I}}\right)^{-1} \\ -\left(\Delta E_{\mathrm{gap}} - \eta_{\mathrm{I}} \mathbf{S} \cdot \mathbf{L}^{\mathrm{I}}\right)^{-1} H_{\mathrm{hop}}^{\dagger} & 0 \end{pmatrix}, \tag{S2}$$

where $\Delta E_{\mathrm{gap}} = \epsilon_{\mathrm{Cr}} - \epsilon_{\mathrm{I}}$. Now, the second-order perturbed Hamiltonian is given by $H_2' =$

$H_2^0 + [S, V]/2$, which is a block-diagonal. Taking only the upper half block gives the effective Hamiltonian describing the electronic states in Cr atoms.

$$\begin{aligned} H'_{\mathrm{Cr}} &= H_{\mathrm{Cr}} + H_{\mathrm{hop}}\left(\Delta E_{\mathrm{gap}} - \eta_{\mathrm{I}}\mathbf{S}\cdot\mathbf{L}^{\mathrm{I}}\right)^{-1} H_{\mathrm{hop}}^{\dagger} \\ &\approx \left(H_{\mathrm{Cr}} + \frac{H_{\mathrm{hop}}H_{\mathrm{hop}}^{\dagger}}{\Delta E_{\mathrm{gap}}}\right) + \eta_{\mathrm{I}}\frac{H_{\mathrm{hop}}\mathbf{S}\cdot\mathbf{L}^{\mathrm{I}}H_{\mathrm{hop}}^{\dagger}}{\Delta E_{\mathrm{gap}}^2}. \end{aligned} \tag{S3}$$

At the second step, we neglect higher order contributions from η_{I}. Since the H_{hop} describes spatial hopping of electrons, we assume that the hopping process preserves the spin and angular momentum expectation values. Thus, it can be reasonably approximated by the hoping integral: $H_{\mathrm{hop}} \approx t$. As a result, the second term in Eq. (S3) gives an indirect SOC Hamiltonian with an effective SOC parameter $\xi_2 \sim \eta_{\mathrm{I}}|t|^2/\Delta E_{\mathrm{gap}}^2$. Since ΔE_{gap} is the largest energy scale as seen in Figure 1b, one may treat ξ_2 perturbatively.

To complete our analysis, we present the total magnetic anisotropy energy (MAE) from the direct and the indirect SOCs by using the perturbation theory[1] with respect to each of ξ_i.

$$\begin{aligned} \mathrm{MAE} = \xi_1^2 \sum_{u,o,\sigma,\sigma'} \sigma\sigma' \frac{\left|\langle o,\sigma|L_z^{\mathrm{Cr}}|u,\sigma'\rangle\right|^2 - \left|\langle o,\sigma|L_x^{\mathrm{Cr}}|u,\sigma'\rangle\right|^2}{E_{u,\sigma} - E_{o,\sigma'}} \\ + \xi_2^2 \sum_{u,o,\sigma,\sigma'} \sigma\sigma' \frac{|\langle o,\sigma|L_z^{\mathrm{I}}|u,\sigma'\rangle|^2 - |\langle o,\sigma|L_x^{\mathrm{I}}|u,\sigma'\rangle|^2}{E_{u,\sigma} - E_{o,\sigma'}}, \end{aligned} \tag{S4}$$

where the first and the second term are the direct (Cr) and indirect (I) SOC contribution to the MAE, respectively. As argued in the main text and presented in the next section, the orbital angular momentum mainly originates from I atoms, and thus the first term in Eq. (S4) is negligible. Our discussion in the main text is based on the second term, which is presented as Eq. (1) in the main text. The comparison between the two SOCs is consistent with the first principles calculations in the previous literature[2].

Atomic character and spin/orbital angular momentum in the CrI_3 monolayer

We investigated the electronic structure of the CrI_3 monolayer. As shown in Figure S1a, the conduction bands are mainly composed of Cr *d*-orbitals, whereas the Cr and I states are mixed in the valence bands. The valence-band edge is unambiguously derived from the I states. To reveal the dominant component of the angular momentum, we replotted the orbital angular momentum of Figure 1b using the normalized value defined as $L_z/[L_x^2 + L_y^2 + L_z^2]^{1/2}$. The normalized orbital angular momentum indicates the predominance of the *z*-direction component. We also calculated the band structure of the CrI_3 monolayer with the in-plane magnetization (Figure S1c), which is essentially the same as the Na adsorption except for the Fermi level shift (Figure 2b). We also confirmed that the orbital angular momentum presented in Figure 1b mainly originates from I atoms by plotting the orbital angular momentum calculated from *p* orbitals (Figure S1d).

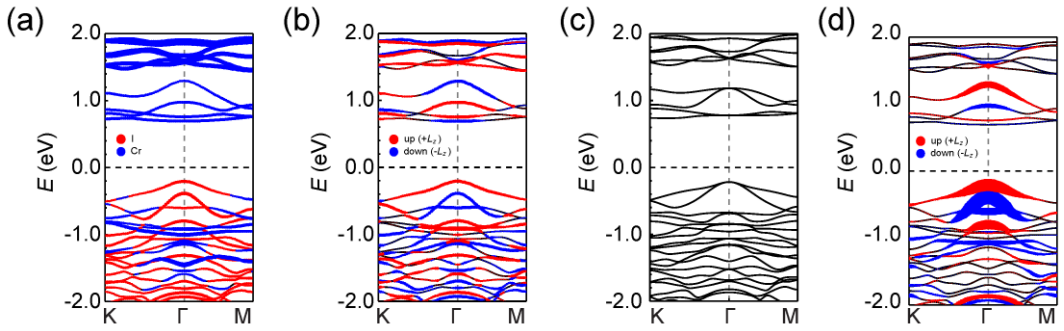

Figure S1. (a) The atom-projected band structure of the CrI_3 monolayer. The contribution of I (Cr) is represented in red (blue). (b) The calculated band structure of the CrI_3 monolayer with the normalized orbital angular momentum defined as $L_z/[L_x^2 + L_y^2 + L_z^2]^{1/2}$. Orbital-up (orbital-down) states are marked by red (blue) dots. (c) The calculated band structure of the CrI_3 under the in-plane magnetization. (d) The I-*p* orbitals contribution to the orbital angular momentum, implying that the orbital angular momentum mainly originates from I atoms.

Static correlation effect on the electronic structure

We investigated the effect of the static correlation on the electronic structure via the on-site Coulomb potential (U = 2.65 eV on 3d orbitals of Cr atom). The unique angular momentum distributions of the CrI_3 were retained even though the U effect was considered, as shown in Figure S2.

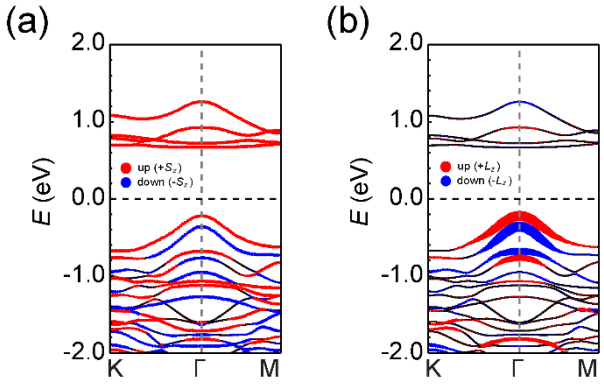

Figure S2. The calculated band structure of the CrI_3 monolayer with (a) the spin angular momentum and (b) the orbital angular momentum under the generalized gradient approximation (GGA)+U scheme. Spin-up (orbital-up) and spin-down (orbital-down) states are marked by red and blue dots, respectively.

Magnetic anisotropy energy change by various adsorbates

We examined the variation in the magnetic anisotropy energy (MAE) induced by atomic adsorption. We tested group 13 and 14 elements as well as alkali and alkaline-earth elements. For the group 13 and 14 elements, adsorbates cannot penetrate into the midst (Figure S5a), and from bonding with iodine atoms the MAEs are mostly negative (Figure S3b). Even the *s* orbitals of alkaline-earth atoms severely hybridize with the CrI_3 monolayer, leading to the prominent peak at around -5 eV in the density of states. When the magnetization of Pb-adsorbed CrI_3 layer is configured into the *z*-direction, the CrI_3 layer has a nonzero Chern number (C = 2). The singular band cross can be inferred from the bands near the K point (Figure S3d), and the non-vanishing Berry curvature is indeed observed (Figure S3e). However, the CrI_3 has an in-plane easy axis when a Pb atom is placed on it; thus, a Chern insulator cannot be realized in the CrI_3 monolayer.

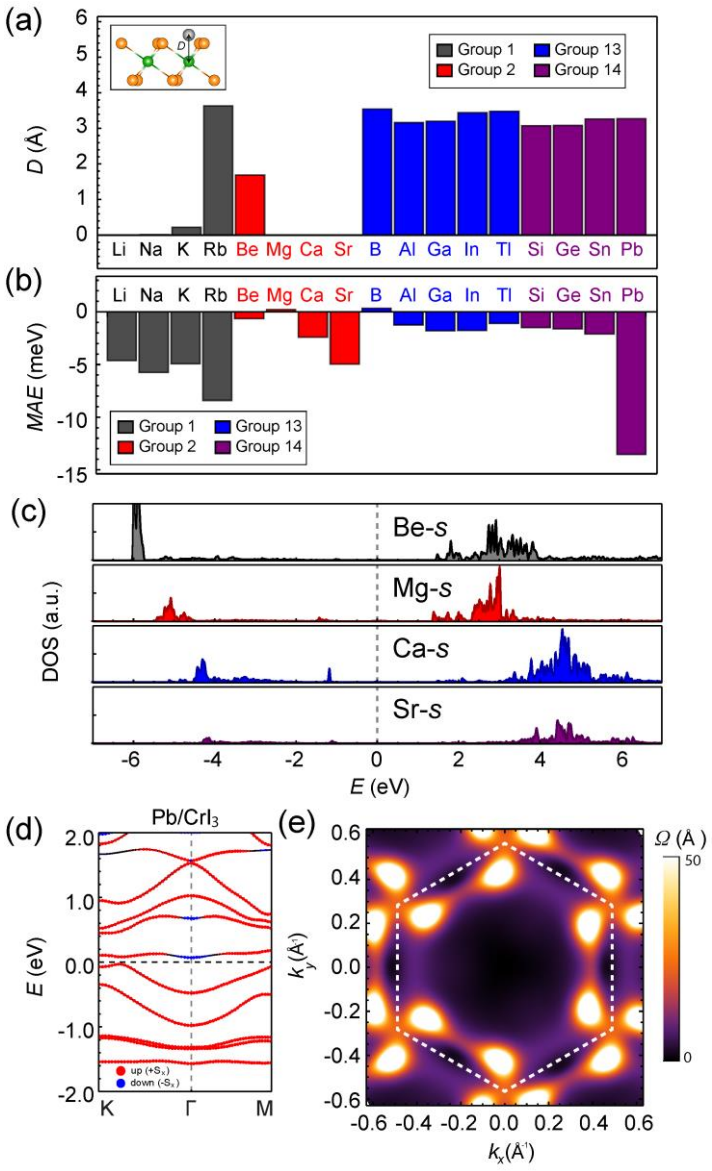

Figure S3. (a) The optimized distance (D) between the adsorbate and the Cr plane of CrI_3 (upper panel) and (b) corresponding magnetic anisotropy energy (MAE) (lower panel). (c) The calculated density of states (DOS) of the *s* orbital of the alkaline-earth adsorbate. (d) The calculated electronic structure of the CrI_3 monolayer with the Pb adatom. Spin-up (spin-down) states are marked by red (blue) dots. (e) The calculated Berry curvature (BC) map in the first Brillouin zone (dashed white lines).

Effect of 3*d* transition metal substitutional doping on magnetic properties

We explored the effect of 3*d* transition metal substitutional doping in the CrI_3 monolayer. As the atomic number of a dopant increases, its local magnetic moment increases and reaches the maximum value at the Mn or Fe atomic number, followed by a monotonic decrease. The exchange energy, defined as the energy difference between the ferromagnetic and the antiferromagnetic ordering, is positive and thus ferromagnetism is favored when the dopant is lighter than Cr. For the dopants heavier than Cr, antiferromagnetic ordering is preferred. The results of Co doping delicately depend on the on-site Coulomb potential, while for other elements the GGA results are largely consistent with those of the GGA+*U*.

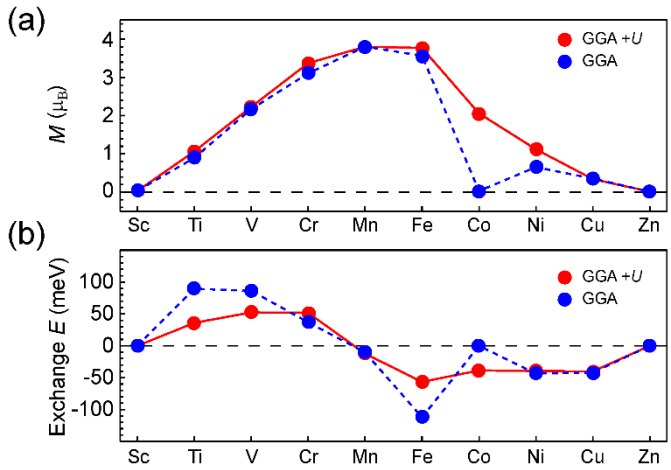

Figure S4. The variation of (a) the magnetic moment and (b) the exchange energy of the CrI_3 monolayer when a Cr atom is replaced by a 3*d* transition metal. The GGA+*U* calculations were performed with U=2.6 eV on the *3d* orbitals.

Magnified view of the real-time profile of the excited state

Here, we present a zoomed-in view of the majority e_g peak around 1 eV in the real-time profile of the excited state to reveal the variation of the electron population of the e_g states with time.

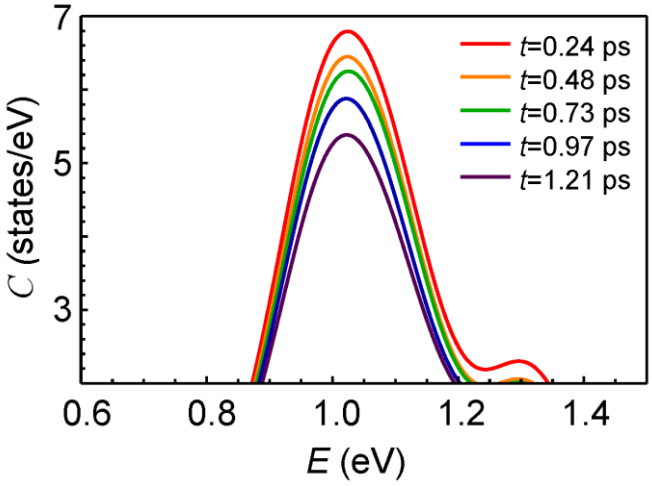

Figure S5. The zoomed-in window for the real-time profile of the projection of the excited state on the ground state.

Real-time TDDFT calculation with a light frequency of 2.23 eV

The projected density of states (Figure 4b) and the dielectric constant (Figure 4a) imply that the light with the frequency range of 2~3 eV would induce similar excitation. Here, we performed the same real-time time-dependent DFT calculation with alight frequency of 2.23 eV. The time-evolving profiles of electronic structure and the magnetization indeed reveal qualitatively the same results as that in Figure 4.

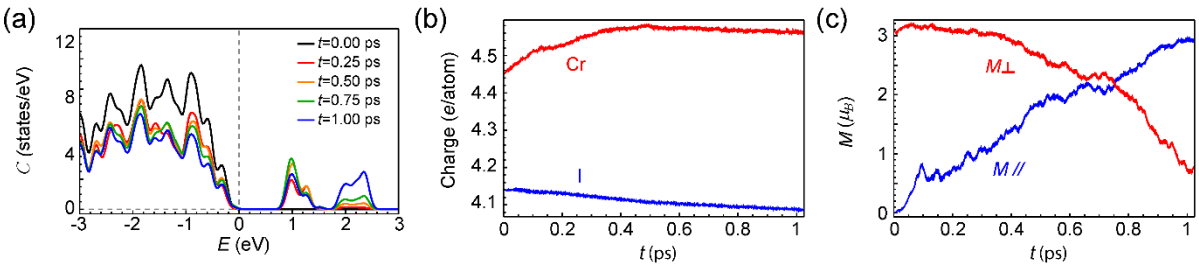

Figure S6. (a) The time-evolving projection of excited states on the ground states. (b) The variation of the atomic charges as a function of time. The atomic charge of Cr (I) is denoted by a red line (blue line) (c) The variation of the magnetic moment as a function of time. The out-of-plane ($M_{\perp}$) and in-plane ($M_{//}$) contributions are denoted by red and blue lines, respectively.

Effect of lattice mismatch in the CrI_3/graphene bilayer

We examined the effect of lattice mismatch in the CrI3/graphene bilayer on the MAE (Figure S7). Two independent geometry optimizations revealed that 5×5 graphene cell is 1.6% larger than $\sqrt{3} \times \sqrt{3}$ cell of the graphene. To assess the effect of strain coming from the lattice mismatch (1.6 %), we calculate the MAE in the 2% stretched CrI_3 varying the number of occupied electrons. The trend of MAE is well preserved. We also checked the effect of I displacement on the MAE that can be caused by the contact with graphene layer. The variation of the MAE is not large in the moderate displacement (< 2 %) and the electronic structure is robust against large I displacements (8 %). We conclude that the effect of the lattice mismatch on the MAE in the CrI3/graphene bilayer is very marginal.

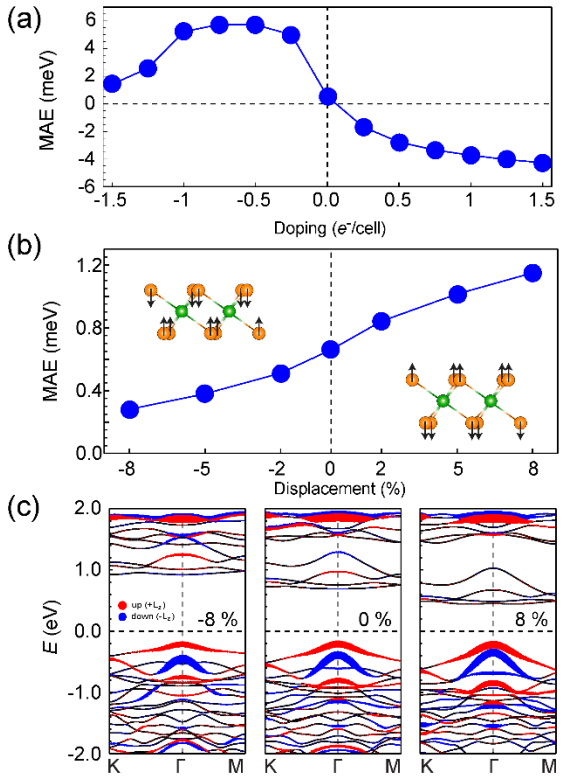

Figure S7. (a) The calculated magnetic anisotropy energy (MAE) of the CrI_3 monolayer 2 % stretched in the lateral direction with various doping levels. (b) The variation of the MAE as a function of I displacement along the out-of-plane direction. Cr and I atoms are denoted by green and orange spheres, respectively. (c) The band structure of the CrI_3 monolayer stretched

(8 %) or compressed (-8 %) along the out-of-plane direction.

Reference

(1) Wang, D.; Wu, R.; Freeman, A. J. First-Principles Theory of Surface Magnetocrystalline Anisotropy and the Diatomic-Pair Model. *Phys. Rev. B* **1993**, *47* (22), 14932.

(2) Lado, J. L.; Fernández-Rossier, J. On the Origin of Magnetic Anisotropy in Two Dimensional CrI3. *2D Mater.* **2017**, *4* (3), 035002.